Dyes and Pigments 92 (2012) 1384–1393

Contents lists available at SciVerse ScienceDirect

Dyes and Pigments

journal homepage: www.elsevier.com/locate/dyepig

New diketo-pyrrolo-pyrrole (DPP) sensitizer containing a furan moiety for efficient and stable dye-sensitized solar cells

Sanyin Qu, Bing Wang, Fuling Guo, Jing Li, Wenjun Wu*, Cong Kong, Yitao Long, Jianli Hua*

Key Laboratory for Advanced Materials and Institute of Fine Chemicals, East China University of Science & Technology, 130 Meilong Road, Shanghai 200237, PR China

ARTICLE INFO

Article history:
Received 21 June 2011
Received in revised form
8 September 2011
Accepted 12 September 2011
Available online 22 September 2011

Keywords:
Diketo-pyrrolo-pyrrole
Metal-free
Dye-sensitized solar cell
Furan
Ionic liquid electrolyte
Stability

ABSTRACT

A new metal-free organic sensitizer containing a furan moiety as the π-spacer based on the diketo-pyrrolo-pyrrole unit was synthesized through simple synthetic routes and with low cost for the application of dye-sensitized solar cells. Two corresponding dyes with benzene and thiophene spacers were also synthesized for the purpose of comparison. On the basis of optimized DSSC test conditions, the sensitizer containing the furan shows prominent solar energy conversion efficiency (η) of 5.65% (J_{sc} = 15.96 mA cm^{-2}, V_{oc} = 541 mV, ff = 0.65) under simulated full sunlight irradiation. The dyes were also tested in a solvent-free ionic liquid electrolyte devices and the stability of devices was performed over 2000 h at full sunlight. The sensitizer containing the furan moiety exhibited good stability and better photovoltaic performance of up to 4.41% power conversion efficiency.

1. Introduction

The ever-increasing demands for renewable energy sources have led to intense research on a variety of light-harvesting devices. Among these, dye-sensitized solar cells [1] have attracted much attention as a promising, efficient, molecular photovoltaic device. At present, DSSCs based on Ru (II)-polypyridyl complexes have an overall solar energy conversion efficiency (η) approaching 12% in small area [2] and with a module efficiency exceeding 8% [3] under simulated AM 1.5 irradiation (100 mW cm^{-2}). On the other hand, metal-free organic dyes have also been developed for DSSCs due to their high molar absorption coefficient, simple synthesis process and structure adjustability. Recently, novel organic dyes based on cyanine [4], merocyanine [5], coumarin [6], carbazole [7], indoline [8], hemicyanine [9], oligoene [10], xanthene [11], phenothiazine [12] and phenoxazine [13] have been investigated as sensitizers for DSSCs, and solar cells based on triphenylamine and dithienosilole have been reported [14] with an energy conversion efficiency exceeding 10%. However, at present, the photovoltaics sector is still dominated by Si and there has been rare production of DSSCs on a large scale. The bottleneck in the further practical application of DSSCs is the lifetime and cost of the cells [15].

Though many factors control the lifetime and cost of the cells, a crucial element in DSSCs, the sensitizer exerts a significant influence on these two points. In order to improve the cells' stability, several effective strategies, such as introducing oligothiophene linkers [16], starburst carbazole antenna donors [17] and thermally and photochemically stable fluorophores [18] into the sensitizers, are employed in DSSCs. The holes in these dye-sensitizers were delocalized over the large moieties instead of a specific atom, thus avoid forming a localized radical center and thus show relatively good stability [19]. Diketo-pyrrolo-pyrrole (DPP) and some of its derivatives are commercialized pigments with a large fluorophore and exceptional light, weather and heat stability. In our previous studies [20], we have introduced DPP into DSSCs and achieved relatively high efficiency. Since triphenylamine and DPP are both commercially available compounds with low cost, also with the good stability of the DPP fluorophore, making them promising pigments for practical application, therefore it is meaningful to further expand the DPP series of dyes.

As reported so far, most of the metal-free dye-sensitizers with high efficiency rely on thiophene or thiophene-based heterocycles as the π-spacer. In particular, some of the dyes based on coumarin-thiophene dye [21], carbazole-oligothiophene dye [19] and benzothiadizole-thiophene dye [22] show good stability. This could be explained by the fact that holes in such dyes were located on the thiophene moieties. And furan, thiophene's oxygen analog, which has a higher oxidation potential, would be more efficient for the

* Corresponding authors. Tel.: +86 21 64250940; fax: +86 21 64252758.
E-mail addresses: wjwu@ecust.edu.cn (W. Wu), jlhua@ecust.edu.cn (J. Hua).

0143-7208/$ – see front matter © 2011 Elsevier Ltd. All rights reserved.
doi:10.1016/j.dyepig.2011.09.009

hole location and reinforce the stability of the dye-sensitizers [19,23]. However, furan has received much less attention compared to the thiophene unit. Recently, furan units have also been incorporated into some conjugated polymers and oligomers as an alternative to thiophenes for photovoltaics and have revealed that the optical and charge carrier mobility can be quite comparable to that of thiophenes [24]. Small chromophores containing a furan unit applied in dye-sensitized solar cells have also been reported and showed relatively high efficiency [25]. There have been reports showing that the incorporation of a furan moiety can somewhat improve polymer solubility substantially and gain high molecular weight [26]. The introduction of a furan moiety in DPP-based dye-sensitizers and compared with other π-spacer would be interesting. More importantly, furan derivatives can be synthesized from a variety of natural products; hence, the dye-sensitizers based on furan can be considered as the renewable and sustainable synthetic resources and allow for production of DSSCs at a large scale [26,27].

Based on the above consideration, we have designed and synthesized a new DPP-based organic sensitizer **DPP-I** containing a furan moiety as a π-spacer, and the corresponding dyes **DPP-II** and **DPP-III** with a benzene and a thiophene π-spacer for the purpose of comparison were designed and synthesized; corresponding molecular structures of the three dyes are shown in Scheme 1. The sensitizers have been applied to sensitization of nanocrystalline TiO_2-based solar cells and the effect of π-spacer linkers on light absorption, energy level, photocurrent and photovoltage will be detailed in this paper.

2. Experimental section

2.1. Equipment

NMR spectra were obtained on Brücker AM 500 spectrometer. The absorption spectra of the dyes in solution and adsorbed on TiO_2 films were measured with a Varian Cary 500 spectrophotometer. MS were recorded on ESI mass spectroscopy. The cyclic voltammograms of dyes were obtained with a Versastat II electrochemical workstation (Princeton applied research) using a normal three-electrode cell with a Pt working electrode, a Pt wire counter electrode, and a regular calomel reference electrode in saturated KCl solution. The supporting electrolyte was 0.1 M $TBAPF_6$ (tetra-n-butylammonium hexafluorophosphate) in acetonitrile/THF(3:1, v/v) as the solvent.

2.2. Materials

Optically transparent FTO conducting glass (fluorine doped SnO_2, transmission >90% in the visible, sheet resistance 15 Ω/square) was obtained from the Geao Science and Educational Co. Ltd. of China and cleaned by water, acetone, distilled water and ethanol in turn. TiO_2 paste was purchased from Solaronix (Switzerland). Lithium iodide was obtained from Fluka. Tetrahydrofuran (THF) was pre-dried over 4 Å molecular sieves and distilled under argon atmosphere from sodium benzophenoneketyl immediately prior to use. Dichloromethane and pyridine were distilled under normal pressure and dried over calcium hydroxide. Starting material 3-[4-[4-(N,N-bis(4-methoxyphenyl)amino)phenyl]pheny-l]-6-(4-bromophenyl)-2,5-di-n-butyl-pyrrolo [3,4-c]pyrrole-1,4-dione (**1**) was synthesized according to our previous studies [20]. **DPP-III**, included for comparison, was synthesized in our earlier studies [20]. All other chemicals were purchased from Aldrich and used as received without further purification.

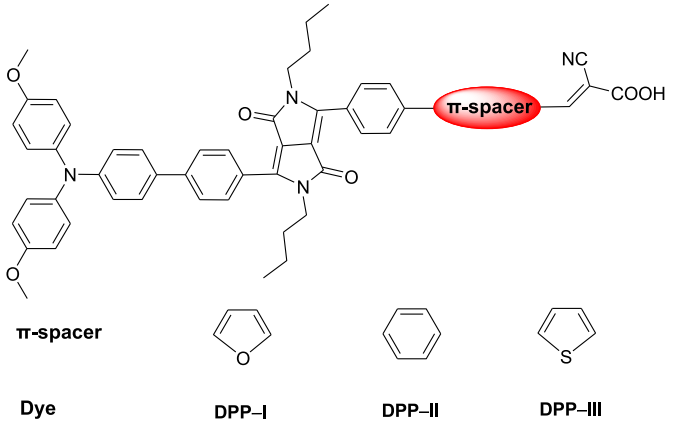

Scheme 1. Molecular structures of dyes **DPP** (**I** ~ **III**).

2.3. Preparation of solar cells

A screen-printed TiO_2 particle was used as photoelectrode. The thickness of TiO_2 film was controlled by the mesh size of screen printing with different layers and measured by a surface profile (Dektak Co., Model DAKTAK **II**). Sintering was carried out at 450 °C for 30 min. Before immersion in the dye solution, these films were soaked in the 0.2 M aqueous $TiCl_4$ solution overnight in a closed chamber and washed with water and ethanol, which can significantly increase the short circuit photocurrent. Then the films were heated again at 450 °C for 30 min followed by cooling to 80 °C and dipping into a 3×10^{-4} M solution of dyes in dichloromethane for 12 h at room temperature. To prepare the counter electrode, the Pt catalyst was deposited on the cleaned FTO glass by coating with a drop of H_2PtCl_6 solution (0.02 M in 2-Propanol solution) with the heat treatment at 400 °C for 15 min. A hole (0.8-mm diameter) was drilled on the counter electrode by a Drill-press. The perforated sheet was cleaned by ultrasound in an ethanol bath for 10 min. About the assemblage of DSSCs, the dye-covered TiO_2 electrode and Pt-counter electrode were assembled into a sandwich type cell and sealed with a hot-melt gasket of 25 μm thickness made of the ionomer Surlyn 1702 (Dupont). The size of the TiO_2 electrodes used was 0.28 cm^2. A drop of the electrolyte was put on the hole in the back of the counter electrode. It was introduced into the cell via vacuum backfilling. Finally, the hole was sealed using a UV-melt gum and a cover glass (0.1 mm thickness). The electrolyte employed was a solution of 0.6 M PMII (1-propyl-3-methyl imidazolium iodide), 0.1 M LiI, 0.05 M I_2, in a mixture of acetonitrile andmethoxypropionitrile(volume ratio, 7:3). For the solvent-free ionic liquid electrolyte, which consists of 1-butyl-3-methyl imidazolium, iodine, benzimidazole and guanidine thiocyanate (BMII:I_2:BI:GNCS = 40:1.67:0.67:3.33).

2.4. Photoelectrochemical measurements

The photocurrent action spectra were measured with a Model SR830 DSP Lock-In Amplifier, a Model SR540 Optical Chopper (Stanford Research Corporation, USA), a 7IL/PX150 xenon lamp with power supply and a 7ISW301 Spectrometer. The irradiation source for the photocurrent density–voltage (J–V) measurement is an AM 1.5 solar simulator (91160, Newport Co., USA). The incident light intensity was 100 mW cm^{-2} calibrated with a standard Si solar cell. The tested solar cells were masked to a working area of 0.159 cm^2. Volt-current characteristic were performed on the Model 2400 Sourcemeter (Keithley Instruments, Inc. USA). The electrochemical impedance spectroscopy (EIS) measurements of all the DSSCs were performed using a Zahner IM6e Impedance Analyzer (ZAHNER-Elektrik GmbH &CoKG, Kronach, Germany). The frequency range is 0.1 Hz–100 kHz. The applied voltage bias is −0.60 V. The magnitude of the alternating signal is 5 mV.

2.5. Synthesis

2.5.1. Synthesis of 5-[4-[3-[4-(4-(N, N-bis (4-methoxyphenyl) amino) phenyl) phenyl]-2,5-di-n-butyl-pyrrolo [3,4-c]pyrrole-1,4-dione] phenyl]furan-2-carbaldehyde (**2**)

Compound **1** (0.20 g, 0.25 mmol), $Pd(PPh_3)_4$ (10 mg, 0.01 mmol), and Na_2CO_3 (1.02 g, 0.01 mol) in THF (10 mL) and H_2O (5 mL) were heated to 45 °C under a nitrogen atmosphere for 30 min. A solution of 5-formylfuran-2-ylboronic acid (0.070 g, 0.50 mmol) in THF (5 mL) was added slowly, and the mixture was heated under reflux for further 12 h. After cooling to room temperature, the mixture was extracted with CH_2Cl_2 (30 mL). The organic portion was combined and removed by rotary evaporation. The residue was purified by column chromatography on silica (CH_2Cl_2/ethyl acetate = 1/70, v/v) to give a red solid. (Yield: 78.5%). mp 115–117 °C. IR (KBr): 2953, 2931, 1671, 1606, 1503, 1245, 1099, 1030, 823. ^{1}H NMR ($CDCl_3$, 500 MHz) δ: (ppm) 9.69 (s, 1H), 7.95 (d, J = 8.8 Hz, 2H), 7.92 (d, J = 9.2 Hz, 2H), 7.89 (d, J = 8.4 Hz, 2H), 7.69 (d, J = 8.4 Hz, 2H), 7.46 (d, J = 8.8 Hz, 2H), 7.34 (d, J = 4.0 Hz, 1H), 7.10 (d, J = 8.4 Hz, 4H), 6.98 (d, J = 8.4 Hz, 2H), 6.94 (d, J = 3.6 Hz, 1H), 6.86 (d, J = 8.8 Hz, 4H), 3.81 (m, 10H), 1.61 (m, 4H), 1.29 (m, 4H), 0.87 (m, J = 7.2 Hz, 7.2 Hz, 6H).^{13}C NMR ($CDCl_3$, 125 MHz) δ: (ppm) 177.4, 171.1, 162.9, 162.6, 158.2, 156.2, 152.5, 149.0, 146.5, 143.7, 140.5, 131.1, 130.9, 129.3, 127.6, 127.0, 126.5, 125.8, 125.5, 120.1, 114.8, 110.6, 109.6, 109.1, 68.0, 60.4, 55.5, 42.0, 41.9, 31.6, 31.6, 25.6, 21.1, 20.0, 14.2, 13.6.

2.5.2. Synthesis of 5-[4-[3-[4-(4-(N, N-bis (4-methoxyphenyl) amino)phenyl) phenyl]-2,5-di-n-butyl-pyrrolo [3,4-c]pyrrole-1,4-dione] phenyl]benzene-2-carbaldehyde(**3**)

Compound **1** (0.20 g, 0.25 mmol), $Pd(PPh_3)_4$ (10 mg, 0.01 mmol), and Na_2CO_3(1.02 g, 0.01 mol) in THF (10 mL) and H_2O (5 mL) were heated to 45 °C under a nitrogen atmosphere for 30 min. A solution of 4-formylphenylboronic acid (0.075 g, 0.50 mmol) in THF (5 mL) was added slowly, and the mixture was heated under reflux for further 12 h. After cooling to room temperature, the mixture was extracted with CH_2Cl_2 (30 mL). The organic portion was combined and removed by rotary evaporation. The residue was purified by column chromatography on silica (CH_2Cl_2/ethyl acetate = 1/70, v/v) to give a red solid. (Yield: 53.4%). mp 101–103 °C. IR (KBr): 2956, 2932, 1655, 1598, 1507, 1246, 1096, 1028, 827. ^{1}H NMR (500 MHz, $CDCl_3$) δ: (ppm) 10.09 (s, 1H), 7.98 (m, J = 8.4 Hz, 8.4 Hz, 4H), 7.91 (d, J = 8.4 Hz, 2H), 7.81 (t, J = 5.6 Hz, 6.0 Hz, 4H), 7.72 (d, J = 8.4 Hz, 2H), 7.48 (d, J = 8.8 Hz, 2H), 7.11 (d, J = 8.8 Hz, 4H), 7.01 (d, J = 8.8 Hz, 2H), 6.87 (d, J = 8.8 Hz, 4H), 3.83 (m, 10H), 1.65 (m, 4H), 1.33 (m, 4H), 0.88 (t, J = 7.2 Hz, 7.6 Hz, 6H). ^{13}C NMR ($CDCl_3$, 125 MHz) δ: (ppm) 191.8, 162.9, 162.7, 148.8, 148.1, 147.4, 143.4, 142.1, 135.7, 133.2, 130.4, 129.4, 129.3, 128.3, 127.8, 127.8, 126.8, 126.3, 124.8, 123.4, 123.3, 110.4, 109.7, 77.4, 77.0, 76.7, 31.7, 31.6, 29.7, 20.1, 13.7.

2.5.3. Synthesis of 2-cyano-3-[5-[4-[3-[4-(4-(N,N-Bis(4-methoxyphenyl)amino) phenyl)phenyl]-2,5-di-n-butyl-pyrrolo [3,4-c]pyrrole-1,4-dione]phenyl]furan-2-yl] acrylic acid (DPP-I)

Compound 2 (0.10 g, 0.12 mmol), 2-cyanoacetic acid (0.11 g, 1.29 mmol), and piperidine (0.5 mL) in THF (20 mL) were heated to reflux under a nitrogen atmosphere for 6 h. After cooling to room temperature, the precipitate was filtered. The residue was purified by column chromatography on silica (CH2Cl2/ethanol = 10/1, v/v) to give a dark red solid. (Yield: 46.3%). mp 241–243 °C. IR (KBr): 3440, 2956, 2933, 2220, 1670, 1591, 1512, 1240, 1091, 1033, 825. ^{1}H NMR (500 MHz, DMSO), δ: 8.09 (d, J = 9.45, 3H), 8.01 (d, J = 8.55, 2H), 7.91 (d, J = 8.46, 2H), 7.81 (d, J = 8.52, 2H), 7.64 (d, J = 8.74, 2H), 7.56 (m, 2H), 7.10 (d, J = 8.90, 4H), 6.96 (d, J = 8.95, 4H), 6.83 (d, J = 8.75, 2H), 3.78 (m, 10H), 1.44 (m, 4H), 1.18 (m, 4H), 0.78 (m, 6H). ^{13}C NMR (125 MHz, DMSO) δ: 165.6, 161.6, 161.4, 157.2, 156.0, 148.7, 148.3, 148.0, 146.0, 142.4, 139.5, 137.5, 130.4, 129.4, 129.3, 129.2, 128.3, 127.4, 127.1, 125.7, 125.3, 124.9, 118.6, 115.0, 111.6, 109.4, 108.6, 55.2, 30.7, 19.2, 19.2, 13.3, 13.3. HRMS (m/z): [M-H]- calcd. for ($C_{54}H_{47}N_4O_7$): 863.3445; found, 863.3445.

2.5.4. Synthesis of 2-cyano-3-[5-[4-[3-[4-(4-(N,N-Bis(4-methoxy phenyl)amino) phenyl)phenyl]-2,5-di-n-butyl-pyrrolo [3,4-c] pyrrole-1,4-dione]phenyl]benzene-2-yl]acrylic acid (DPP-II)

Compound **3** (0.080 g, 0.10 mmol), 2-cyanoacetic acid (0.11 g, 1.29 mmol), and piperidine (0.5 mL) in THF (20 mL) were heated to reflux under a nitrogen atmosphere for 6 h. After cooling to room temperature, the precipitate was filtered. The residue was purified by column chromatography on silica (CH_2Cl_2/ethanol = 10/1, v/v) to give a dark red solid. (Yield: 57.8%). mp 223–225 °C. IR (KBr): 3445, 2962, 2930, 2221, 1650, 1592, 1510, 1380, 1243, 1090, 1041, 823. ^{1}H NMR (500 MHz, DMSO) δ: 8.37 (s, 1H), 8.18 (d, J = 8.04, 2H), 8.00 (m, 8H), 7.84 (d, J = 8.33, 2H), 7.66 (d, J = 8.55, 2H), 7.11 (d, J = 8.63, 4H), 6.96 (d, J = 8.82, 4H), 6.84 (d, J = 8.18, 2H), 3.76 (m, 10H), 1.46 (m, 4H), 1.18 (m, 4H), 0.79 (t, J = 7.13, 7.13, 6H). ^{13}C NMR (125 MHz, DMSO) δ: 165.8, 160.9, 160.6, 156.1, 154.9, 154.2, 152.8, 149.8, 146.8, 146.8, 146.6, 144.5, 141.7, 139.5, 136.9, 129.2, 127.5, 127.2, 125.8, 123.0, 122.6, 122.1, 118.7, 116.5, 115.1, 114.4, 111.4, 109.7, 109.2, 55.2, 30.6, 19.3, 19.2, 13.9, 13.4, 11.3. [M-H]- calcd. for ($C_{56}H_{49}N_4O_6$): 873.3652; found, 873.3662.

3. Results and discussion

3.1. Synthesis

The synthetic routes of the dyes are shown in Scheme 2. **DPP-III** and3-[4-[4-(N,N-bis(4-methoxyphenyl)amino)phenyl]phenyl]-6-(4-bromophenyl)-2,5-di-n-butyl-pyrrolo [3,4-c]pyrrole-1,4-dione (**1**) were obtained as reported earlier [20]. **DPP-I** and **DPP-II** were synthesized by Suzuki coupling reaction of compound 1 with 5-formylfuran-2-ylboronic acid, 4-formylphenylboronic acid, followed by Knoevenagel condensation reaction with cyanoacetic acid. The structure of all of the key intermediates and two novel organic DPP sensitizers have been confirmed by ^{1}H NMR, ^{13}C NMR and HRMS.

3.2. Material

The TiO_2 paste was important part during the preparation of dye-sensitized solar cells. In this study, the TiO_2 paste was purchased from Solaronix (Switzerland) instead of P25 (Degussa) used in the previous studies. Commercial available P25 produced by Degussa (Evonik) is widely used in dye-sensitized solar cells because of its relatively high activity and low cost. However, it is known that P25 is composed of anatase and rutile crystallites [28], and rutile is worse than anatase for solar energy conversion [29]. Thus, P25 is not the best choice for high efficiency dye-sensitized solar cells. The TiO_2 paste purchased from Solaronix (Switzerland) were prepared by sol-gel route and with pure anatase crystallite, which is better for solar energy conversion. It has been reported that those cells with highest solar conversion efficiency (near or higher than 10%) were prepared with TiO_2 paste by sol-gel route [16,30].

3.3. Absorption properties in solutions and on TiO_2 film

Absorption spectra of the three dyes in a diluted solution of dichloromethane are shown in Fig. 1 and their absorption data are listed in Table 1. In the UV–Vis spectra, the dyes exhibit three major prominent bands, appearing at 300–325 nm, 340–425 nm, and 500–550 nm, respectively. The absorption band of 300–325 nm

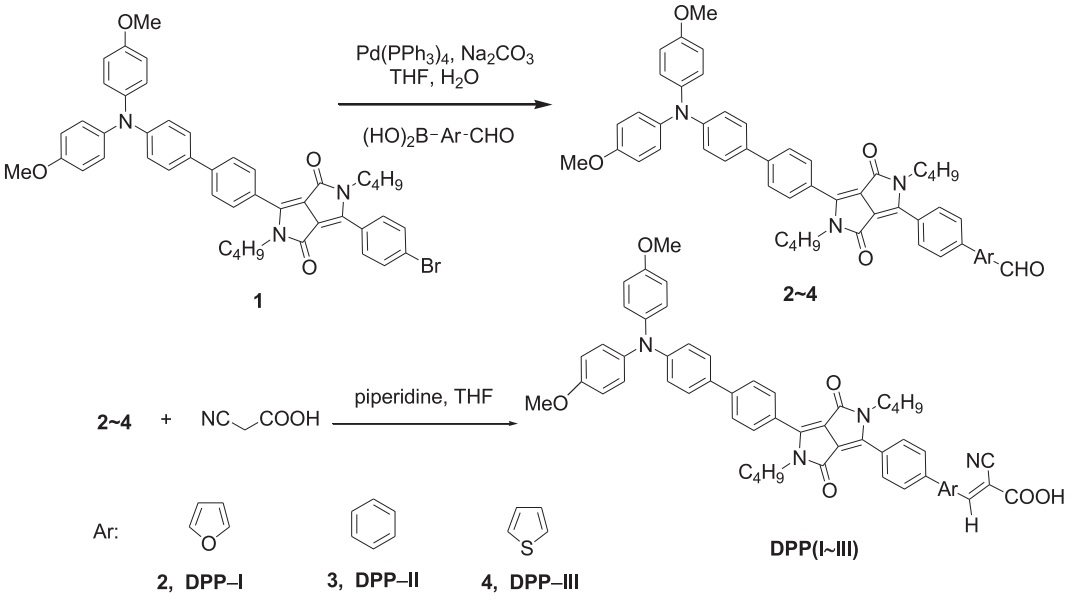

Scheme 2. The synthetic procedure of the dyes **DPP (I ~ III)**.

was ascribed to a localized aromatic π–π* transition of typical triarylamine [31], and the middle band was due to the π–π* transition of diketo-pyrrolo-pyrrole (DPP)-conjugated molecule with the π-spacer of either benzene, furan or thiephene group. Compared with **DPP-I** and **DPP-III**, **DPP-II**. exhibits a middle peak at 343 nm ($\varepsilon = 4.77 \times 10^4$) blue shifted by about 50 nm. This may be caused by the decrease of co-planarity between diketo-pyrrolo-pyrrole (DPP) moiety and the electron acceptor due to the introduction of benzene unit [32]. The bands at around 500–550 nm can be attributed to the intramolecular charge transfer (ICT) between the triphenylamine donor and the acceptor, in which **DPP (I ~ III)** show strong visible band at 525 nm, 511 nm and 524 nm owing to the introduction of diketo-pyrrolo-pyrrole (DPP) group, which could favor light-harvesting in DSSCs. The corresponding long wavelength maximum extinction coefficients of the three dyes are 3.88×10^4, 3.28×10^4 and 4.21×10^4 M^{-1} cm^{-1}, respectively. In comparison with conventional ruthenium complexes (for example, 1.39×10^4 M^{-1} cm^{-1} at 541 nm for N3) [33] the present dye molecules show about three times higher absorption coefficients. The greater maximum absorption coefficients of the organic dyes allow a correspondingly thinner nanocrystalline film, which could benefit DSSCs with ionic liquid electrolyte for better conversion efficiencies [34].

Fig. 2 shows the absorption spectra of **DPP (I ~ III)** on TiO_2 films after 12 h adsorption. As shown in Fig. 2, the absorption peaks for **DPP (I ~ III)** on the TiO_2 film are at $\lambda = 590$, 566 and 589 nm, the absorption bands are red-shifted by 65, 55 and 65 nm compared with the solution spectrum, respectively. The red shifts of the absorption spectra on TiO_2 of **DPP (I ~ III)** could be ascribed to the aggregation or electronic coupling of the dyes on the TiO_2 surface. The interaction between the carboxylate group and the surface Ti^{4+} ions may lead to increased delocalization of the π* orbital of the conjugated framework. The energy of the π* level is decreased by this delocalization, which explains the red shift for the absorption spectra.

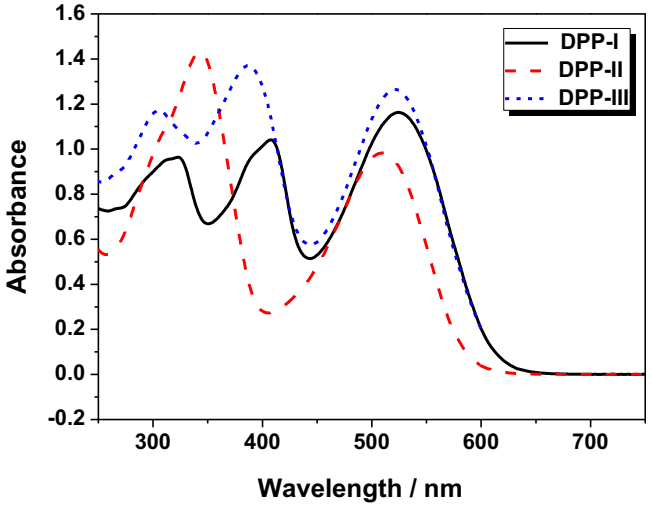

Fig. 1. UV–Vis absorption spectra of **DPP (I ~ III)** in CH_2Cl_2 solution (3×10^{-5} M).

3.4. Electrochemical properties

To evaluate the possibility of electron transfer from the excited

Table 1
Optical properties and redox potential of **DPP (I ~ III)**.

Dye	λ_{max}[a]/nm ($\varepsilon \times 10^{-4}$ M^{-1} cm^{-1})	λ_{max}[b] (nm)	HOMO[c]/V (*vs.*NHE)	E_{0-0}[d] (eV)	LUMO[e]/V (*vs.* NHE)
DPP-I	525 (3.88), 409(3.47), 323 (3.21)	590	0.94	1.95	−1.01
DPP-II	511 (3.28), 343 (4.77), 308 (3.56)	566	0.95	2.01	−1.06
DPP-III	524 (4.21), 388 (4.57), 305 (3.91)	589	1.12	1.91	−0.79

[a] Absorption maximum in CH_2Cl_2 solution (3×10^{-5} M).
[b] Absorption maximum on TiO_2 film.
[c] HOMO were measured in acetonitrile/THF(3:1, v/v) with 0.1 M tetra-n- butylammoniumhexafluorophosphate ($TBAPF_6$) as electrolyte (working electrode: Pt; reference electrode: SCE; calibrated with ferrocene/ferrocenium (Fc/Fc^+) as an external reference. Counter electrode: Pt).
[d] E_{0-0} was estimated from the absorption thresholds from UV–Vis absorption spectra of the dyes.
[e] LUMO is estimated by subtracting E_{0-0} to HOMO.

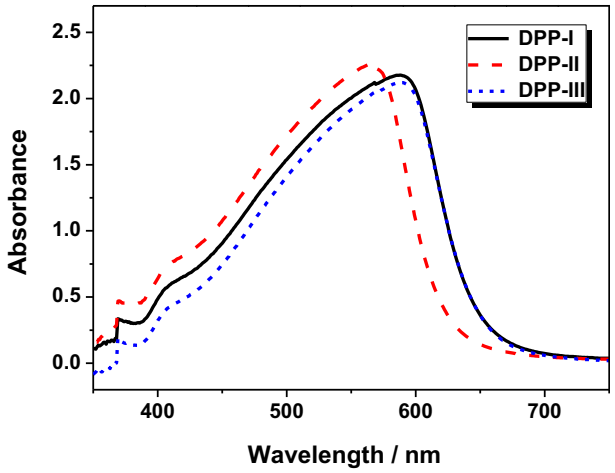

Fig. 2. Absorption spectra of **DPP(I ~ III)** adsorbed on TiO_2 film.

dye to the conduction band of TiO_2, cyclic voltammetry was performed in acetonitrile/tetrahydrofuran solution, using 0.1 M tetrabutylammonium hexafluorophosphate as the supporting electrolyte, Pt as working electrode and counter electrode and saturated calomel electrode (SCE) as reference electrode. The examined highest occupied molecular orbital (HOMO) levels and the lowest unoccupied molecular orbital (LUMO) levels are collected in Table 1. The SCE reference electrode was calibrated using a ferrocene/ferrocenium (Fc/Fc^+) redox couple as an external standard and the $E_{1/2}$ of the Fc/Fc^+ redox couple was found to be 0.37 V versus the SCE reference electrode [12b]. The potentials versus NHE were calibrated by addition of 0.63 V to the potentials versus Fc/Fc^+ [12a]. Therefore, the potentials measured *vs* SCE were converted to normal hydrogen electrode (NHE) by addition of +0.26 V. It can be obtained from the oxidative cyclic voltammetry plot (shown in Fig. 3) that the first half-wave potentials of **DPP (I ~ III)** are 0.68, 0.69 and 0.86 V (vs. SCE). Therefore, the ground state oxidation potential corresponding to the HOMO levels are 0.94, 0.95 and 1.12 V (*vs.* NHE) by addition of 0.26 V, respectively. From Fig. 1, we know that the absorption thresholds for dyes **DPP (I ~ III)** are 636, 616 and 649 nm in CH_2Cl_2 solution, which correspond to the band gap energy (E_{0-0}) of 1.95, 2.01 and 1.91 eV, respectively. The estimated excited-state potential corresponding to the LUMO levels are −1.01, −1.06 and −0.79 V, respectively. The examined HOMO levels and the LUMO levels are listed in Table 1.

The HOMO levels of the three dyes are much more positive than the iodine/iodide redox potential value (0.4 V), ensuring that there is sufficient driving force for efficient dye regeneration through the recapture of the injected electrons from I^- by the dye cation radical. From the LUMO values, all of the three dyes can complete the process of electron injection from the excited dye molecule to TiO_2 conduction band, with a more negative level than the energy level of the TiO_2 electrode (−0.5 V vs. NHE). Furthermore, the energy gaps between the LUMO of the dyes **DPP-I and DPP-II** and TiO_2 conduction band was larger than **DPP-III**, indicating that the electron injection process from the excited dye molecule to TiO_2 conduction band is more efficient [35].

3.5. Photovoltaic performance of liquid electrolyte DSSCs

Fig. 4 shows the action spectra of incident monochromatic photon-to-current conversion efficiency (IPCE) for DSSCs based on **DPP (I ~ III)**. The dye-coated TiO_2 film was used as working electrode, platinized FTO glass as counter electrodes and 0.1 M LiI + 0.05 M I_2 + 0.6 M MPII in acetonitrile and methoxypropionitrile(volume ratio, 7:3) mixture solution as redox electrolyte. The solar cells based on the three dyes exhibit high IPCE values above 60% in the range of 500–600 nm and with the highest value of 83.2% at 535 nm for **DPP-I**, 87.9% at 530 nm for **DPP-II** and 73.5% at 543 nm for **DPP-III**, respectively. By comparison, both of **DPP-I** and **DPP-II** show higher maximum IPCE values and energy conversion efficiencies than the **DPP-III** dye with thiophene unit. The IPCE at a specific wavelength is expressed as

$$IPCE(\lambda) = LHE(\lambda)\phi_{inj}\cdot\eta_c = LHE(\lambda)\cdot\phi(\lambda)_{ET}$$

Where $LHE(\lambda)$ stands for light-harvesting efficiency of the photoelectrode, φ_{inj} is the quantum yield of charge injection from the dye excited-state into TiO_2, η_c is the efficiency of the injected charge collection at the back contact, and $\varphi(\lambda)_{ET}$ is defined as an electron transfer yield, which is a product of the electron injection yield and the charge collection efficiency. Considering similar unity $LHE(\lambda)$ values for all the dyes, higher IPCE values of the

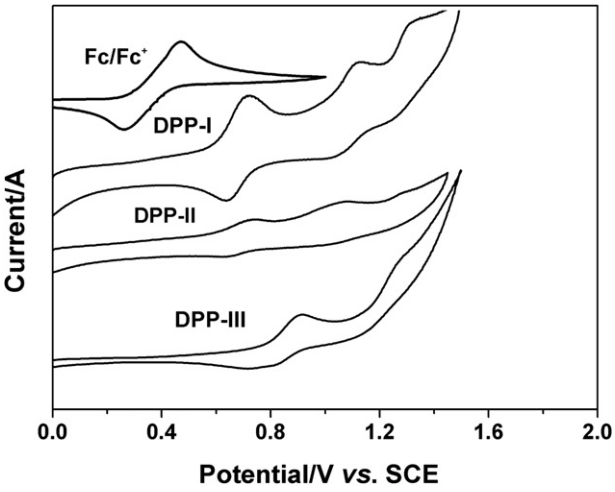

Fig. 3. Cyclic voltammetry plots of **DPP(I ~ III)** in acetonitrile/THF(3:1, v/v).

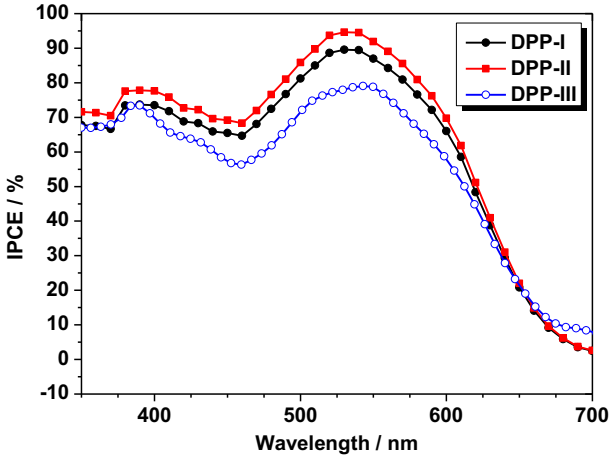

Fig. 4. Photocurrent action spectra of the TiO_2 electrodes sensitized by **DPP (I ~ III)**.

Table 2
Photovoltaic performance of DSSCs based on **DPP (I ~ III)** and N719 dye for 16 μm thick TiO_2 film with liquid electrolyte.

Dye	J_{sc}/mA cm^{-2}	V_{oc}/mV	ff	η (%)	Amount[a] (mol cm^{-2})
DPP-I	12.43	597	0.60	4.43	9.76×10^{-8}
DPP-II	14.53	625	0.66	6.03	1.41×10^{-7}
DPP-III	10.32	567	0.66	3.89	1.12×10^{-7}
N719	16.10	689	0.67	7.47	

[a] Amount of the dyes adsorbed on TiO_2 film.

DSSCs sensitized by the dyes with benzene and furan as π-spacer means that the DSSCs sensitized by the dyes with benzene and furan linkers have higher electron transfer yield $\varphi(\lambda)_{ET}$ than the dye with the thiophene linker. Therefore, the introduction of benzene and furan rings into DPP-based dye structure has a positive effect on IPCE. With judicious molecular structure design to introduce benzene and furan linkers to tune the HOMO-LUMO levels appropriately, higher IPCE thus higher J_{sc} leading to higher energy conversion efficiency could be obtained with these DPP-based dye sensitized solar cells [36].

The current–voltage characteristics of the DSSCs based on 16 μm thickness of TiO_2 film was measured at 100 mW cm^{-2} under simulated AM 1.5G solar light conditions. The **DPP-I**-sensitized cell gave a short circuit photocurrent density (J_{sc}) of 12.43 mA cm^{-2}, an open circuit voltage (V_{oc}) of 0.597 V, and a fill factor of 0.60, corresponding to an overall conversion efficiency of 4.43% (see Table 2). Under the same conditions, the **DPP-II**- and **DPP-III**-sensitized cell gave a J_{sc} of 14.53 and 10.32 mA cm^{-2}, V_{oc} of 0.625 and 0.567 V, and a fill factor (ff) of 0.66 and 0.66, corresponding to an overall conversion efficiency of 6.03% and 3.89%, respectively. **DPP-II** has the highest photocurrent due to more loading, faster and more effective electron injection efficiency. From Fig. 5 and Table 2, we can also see that **DPP-II** has a little higher open circuit voltage than the other two dyes, this could be ascribed to less aggregation occurring for **DPP-II** by the decrease of co-planarity between DPP moiety and the benzene spacer. Compared to **DPP-III**, **DPP-I** has higher photocurrent, indicating that furan moiety may have even better charge carrier mobility than thiophene moiety.

For further optimization of the device performance, the effect of the thickness of the TiO_2 film layer on the performance was carried out, for which Fig. 6 and Table 3 show current–voltage characteristics obtained with DSSCs based on **DPP (I ~ III)** with the thickness ranging from about 8 μm to 23 μm. **DPP-I** yielded a remarkably high photocurrent density (J_{sc}) of 15.96 mA cm^{-2}, open circuit voltage (V_{oc}) of 0.541 V and a fill factor (ff) of 0.65, corresponding to an overall power conversion efficiency (η) of 5.65% based on 13 μm thickness of TiO_2 film and **DPP-III** yielded a high photocurrent density (J_{sc}) of 10.79 mA cm^{-2}, open circuit voltage (V_{oc}) of 0.606 V and a fill factor (ff) of 0.68, corresponding to an overall power conversion efficiency (η) of 4.44% based on 8 μm thickness of TiO_2 film. As can be inferred from Table 3, the photocurrent of **DPP-II**-sensitized solar cell increased with the increasing thickness of TiO_2 nanocrystalline layer at first, when the thickness reached to 16 μm, the solar cell yielded a remarkably high photocurrent density (J_{sc}) of 14.53 mA cm^{-2} under standard global AM 1.5G solar light conditions due to high adsorption. The cell showed an open circuit voltage (V_{oc}) of 0.625 V and a fill factor (ff) of 0.66, corresponding to an overall power conversion efficiency (η) of 6.03%. When the thickness of the TiO_2 film increased from 16 μm to 21 μm, both of the J_{sc} and V_{oc} decreased, this is because the increased surface area also enhanced the possibility for injected electrons to recombine with the I^{3-}electrolyte [37]. Compared to **DPP-II**, **DPP-I** and **DPP-III** achieved their highest efficiency with thinner TiO_2 film, this is ascribed to higher molar extinction coefficient of the two dyes than **DPP-II**.

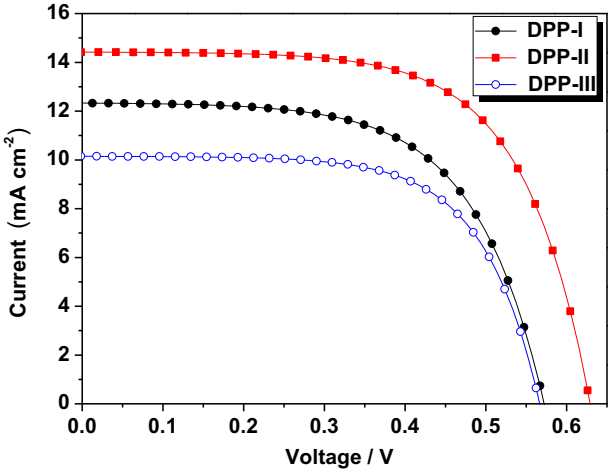

Fig. 5. Current–voltage characteristics of DSSCs based on **DPP(I ~ III)**under irradiation of AM 1.5G simulated solar light (100 mW cm^{-2}) with liquid electrolyte.

3.6. Electrochemical impedance spectroscopy

Electrochemical impedance spectroscopy (EIS) analysis was performed to elucidate the photovoltaic findings further. Fig. 7 showed the electrochemical impedance spectra for the DSSCs based on **DPP (I ~ III)** under a forward bias of −0.60 V in the dark. Three semicircles were observed in the Nyquist plots (Fig. 7(a)). The large semicircle in the Nyquist plots located in the middle is attributed to the dark reaction impedance caused by charge transportation at the TiO_2/dye/electrolyte interface, and the other two small semicircles located in the low- and high- frequency regions are assigned to the charge-transfer at counter electrode and diffusion of I^{3-} in the electrolyte, respectively [38]. The radius of the larger semicircle increases in the order **DPP-III** < **DPP-I** < **DPP-II**, indicating that the electron recombination resistance augments from **DPP-III**, **DPP-I** to **DPP-II** [39]. The electron lifetime values derived from curve fitting are, 23.9, 53.7 and 14.8 ms for **DPP-I**, **DPP-II** and **DPP-III**-sensitized solar cells, respectively. The longest electron lifetime observed with **DPP-II**-sensitized cell indicated there exists efficient suppression of the back reaction of the injected electron with the I^{3-} in the electrolyte, which is reflected in the improvement of the Voc, yielding substantially enhanced device efficiency. At the same time, **DPP-I** exists longer lifetime than **DPP-III**-sensitized cell, indicating that the sensitizer containing the furan moiety may be more efficient for suppression of the back reaction of the injected electron with the I^{3-} in the electrolyte. The Bode phase plots shown in Fig. 7(b) likewise support the differences in the electron lifetime for TiO_2 films derived with the three dyes.

3.7. Photovoltaic performance of solvent-free ionic liquid electrolyte DSSCs

To lower the cost of photovoltaic power production, a substantial improvement in the DSSC efficiency by structure modification is still necessary. Nevertheless, long-term stability is also a vital parameter for sustained cell operation. However, the use of organic solvents is undesirable as they are likely to be volatile, so we

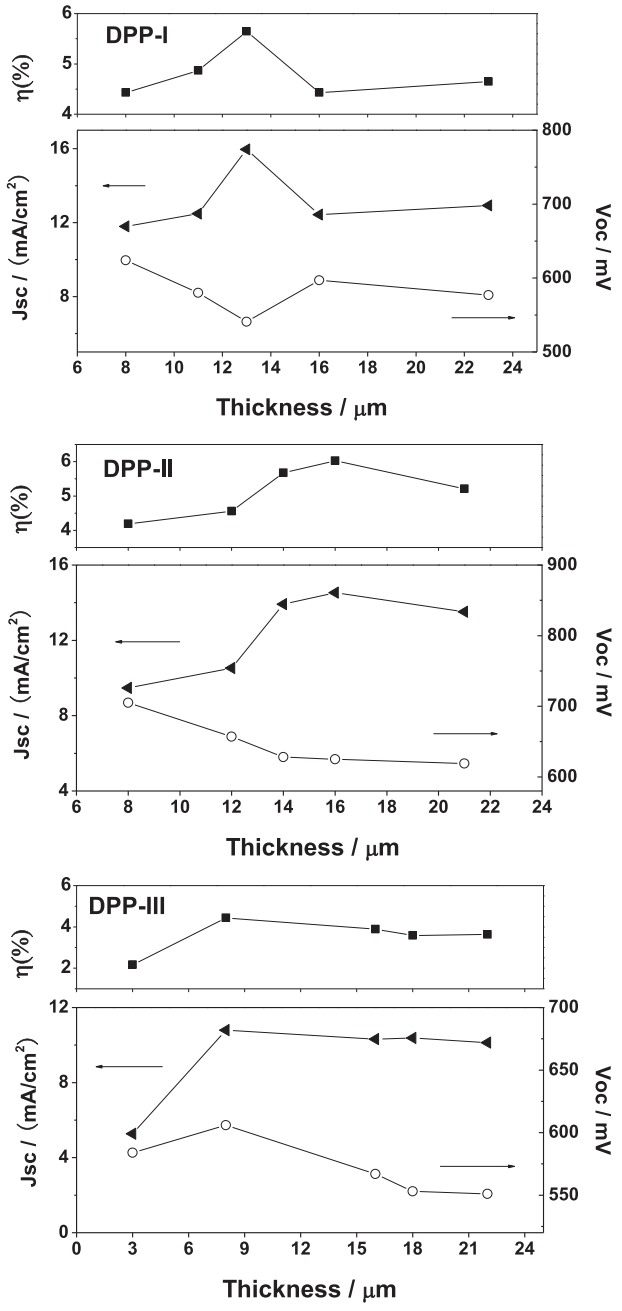

Fig. 6. Current–Voltage characteristics obtained with DSSCs based on **DPP (I ~ III)**with various thicknesses of the nanocrystalline TiO_2 films.

substituted the liquid electrolyte with a solvent-free ionic liquid electrolyte [40]. **DPP (I ~ III)** were evaluated as sensitizers for the solvent-free ionic liquid electrolyte dye-sensitized solar cell using 1-butyl-3-methyl imidazolium, iodine, benzimidazole and guanidine thiocyanate (BMII:I_2:BI:GNCS = 40:1.67:0.67:3.33) as redox electrolyte [41]. Fig. 8(a) shows the incident monochromatic photon-to-current conversion efficiency (IPCE) of **DPP (I ~ III)**-sensitized solar cells with ionic liquid electrolyte based on 8 μm thickness of TiO_2 film. From Fig. 8 (a) we can see that the three dyes can efficiently convert visible-light to photocurrent in the region from 350 to 700 nm. **DPP-I** reaches its maximum of 64.2% at 540 nm, **DPP-II** reaches its maximum IPCE of 53.3% at 530 nm and

Table 3
Current–voltage characteristics obtained with **DPP (I ~ III)**-sensitized solar cells for various thicknesses of the nanocrystalline TiO_2 films.

Dye	Thickness/um	J_{sc}/mA cm^{-2}	V_{oc}/V	FF	η/%
DPP-I	8	11.79	0.624	0.60	4.43
	11	12.48	0.580	0.67	4.87
	13	15.96	0.541	0.65	5.65
	16	12.43	0.597	0.60	4.43
	23	12.92	0.577	0.62	4.65
DPP-II	8	9.47	0.705	0.63	4.19
	12	10.53	0.657	0.66	4.56
	14	13.92	0.628	0.65	5.68
	16	14.53	0.625	0.66	6.03
	21	13.52	0.619	0.62	5.21
DPP-III	8	10.79	0.606	0.68	4.44
	16	10.32	0.567	0.66	3.89
	18	10.38	0.553	0.63	3.59
	22	10.13	0.551	0.65	3.64

DPP-III reaches of 40.5% at 540 nm, respectively. In the spectral range 500–600 nm, the IPCE data of **DPP (I ~ III)** exceed 50%, 60% and 40%, respectively. On the other hand, the IPCE value of **DPP-III** is higher than that for **DPP-II** in the range of 600–700 nm. As a result, the IPCE performance of the ionic liquid electrolyte DSSCs based on **DPP-II** and **DPP-III** is similar. Compared to **DPP-II**, the IPCE value of **DPP-I** is higher while there exists the opposite result in liquid electrolyte. This could be explained by the different thickness of TiO_2 films used in the liquid electrolyte and solvent-

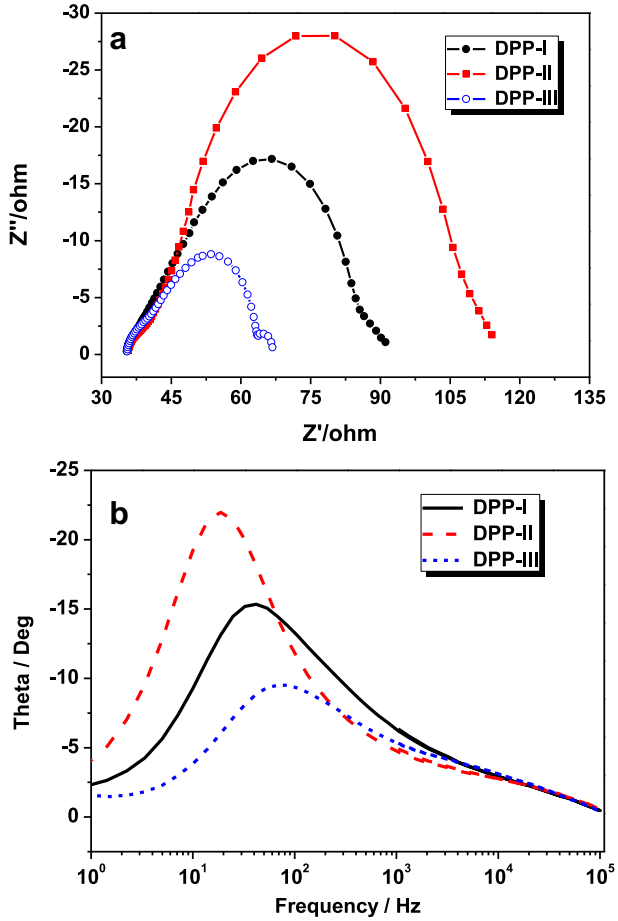

Fig. 7. Impedance spectra of DSSCs based on **DPP (I~III)** measured at -0.60 V bias in the dark. (a) Nyquist plots; (b) Bode phase plots.

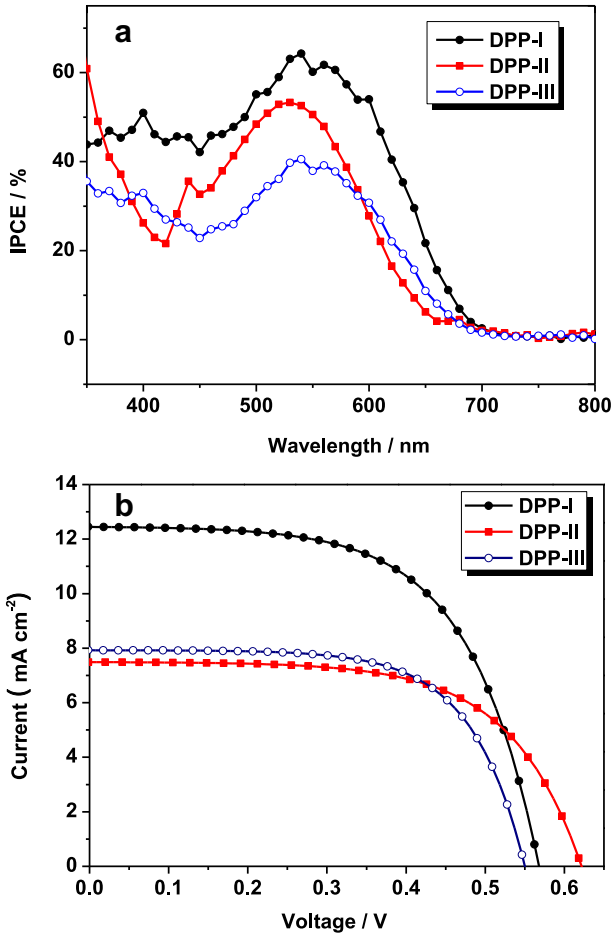

Fig. 8. (a) IPCE and (b) Photocurrent–voltage curves of TiO_2 electrodes obtained with solvent-free ionic liquid electrolyte solar cells sensitizedby dyes with **DPP (I∼III)**.

free ionic liquid electrolyte DSSCs. Since the diffusion of I^- and I^{3-} ions in ionic liquid electrolyte is slow because of their high viscosity, a thin nanocrystalline TiO_2 film is necessary to reach high conversion efficiencies in solvent-free ionic liquid electrolyte DSSCs. For this reason, metal-free organic dyes with high absorption are ideal for solvent-free ionic liquid DSSCs [34]. As a result, **DPP-I** with a furan π-spacer achieved better IPCE performance than **DPP-II**.

Photovoltaic performances of **DPP (I ∼ III)**-sensitized TiO_2 film electrodes with a solvent-free ionic liquid electrolyte under standard global AM 1.5 solar condition (100 mW cm^{-2}) are listed in Table 4, and the corresponding photocurrent-voltage curves are shown in Fig. 8 (b). **DPP-I**-sensitized cell gave a short circuit photocurrent density (J_{sc}) of 12.68 mA cm^{-2}, an open circuit voltage (V_{oc}) of 0.568 V and a fill factor (*ff*) of 0.61, corresponding to an overall conversion efficiency (η) of 4.41% and **DPP-II**-sensitized cell gave a short circuit photocurrent density (J_{sc}) of 7.78 mA cm^{-2}, an open circuit voltage (V_{oc}) of 0.650 V and a fill factor (*ff*) of 0.58, corresponding to an overall conversion efficiency (η) of 2.93%. Under the same conditions, the **DPP-III**-sensitized cell gave J_{sc} values of 8.14 mA cm^{-2}, V_{oc} of 0.549 V and *ff* of 0.68, corresponding to the η of 3.03%. Obviously, **DPP-I** and **DPP-III** show a higher efficiency than **DPP-II** (Table 4). The larger η of

Table 4
Performance parameters of solvent-free ionic liquid electrolyte solar cells sensitized by **DPP (I ∼ III)**.[a]

Dye	J_{sc} (mA cm^{-2})	V_{oc} (V)	ff	η(%)
DPP-I	12.68	0.568	0.61	4.41
DPP-II	7.78	0.650	0.58	2.93
DPP-III	8.14	0.549	0.68	3.03
N719	13.30	0.636	0.67	5.65

[a] Illumination: 100 mW cm^{-2} simulated AM 1.5 G solar light; electrolyte containing: 1-butyl-3-methyl imidazolium, 1-methyl-3-trimethylsilyl imidazolium, iodine, benzimidazole and guanidine thiocyanate(BMII: I_2:BI:GNCS = 40:1.67:0.67:3.33).

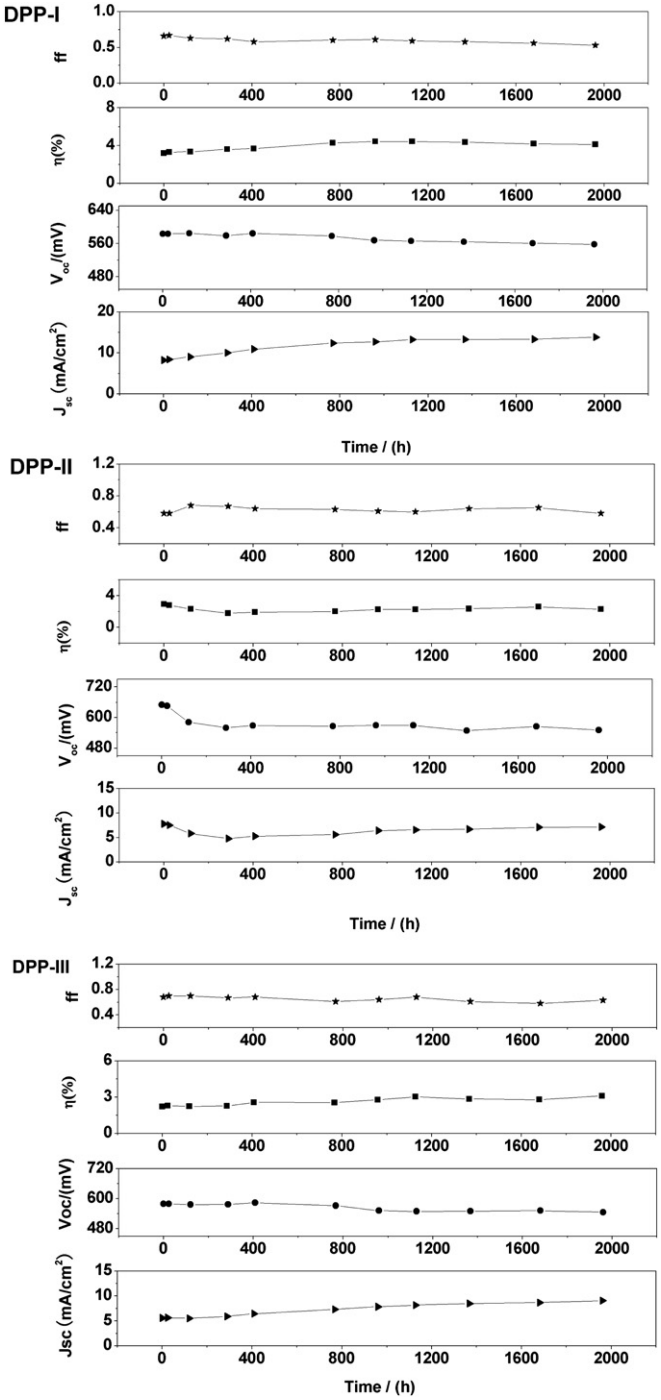

Fig. 9. Stability test photovoltaic parameter (J_{sc}, V_{oc}, ff, and η) variations with aging time for the device based on **DPP (I ∼ III)** and solvent-free ionic liquid electrolyte during successive 1 sun visible-light.

DPP-I and **DPP-III** than **DPP-II** in ionic liquid electrolyte cells can be tentatively attributed to the higher molar extinction and light-harvesting efficiency of the photoelectrode and the prevention of dye aggregates on the semiconductor. In addition, the efficiency in the case of **DPP-III** is lower than that of **DPP-I**, which is ascribed to the reduction of the photocurrent due to the less energy gaps between the LUMO of the dye **DPP-III** and the TiO_2 conduction band. Long-term stability measurements of devices with solvent-free ionic liquid electrolyte were performed over 2000 h at full sunlight. The photovoltaic performance during a long-term accelerated aging of solar cells sensitized with **DPP (I ~ III)** is shown in Fig. 9. Values for the short circuit photocurrent density (J_{sc}), open circuit voltage (V_{oc}), fill factor (ff), and overall efficiency (η) were recorded over a period of 2000 h. On continuous 2000 h of light soaking, the **DPP-I** and **DPP-III-**sensitized solar cells showed an increase of η during the initial 500 h and then remained almost constant for 2000 h. The photocurrents for the two dyes continue to increase under illumination, while the open circuit voltage (V_{oc}) dropped gradually which may be due to an enhancement of the dark current. The short circuit photocurrent (J_{sc}) gain compensates the loss of the open circuit voltage (V_{oc}), resulting in almost constant efficiency of **DPP-I** and **DPP-III-**sensitized solar cells during light soaking. As for the **DPP-II-**sensitized solar cell, the short circuit photocurrent (J_{sc}) and open circuit voltage (V_{oc}) decreased sharply for the first 500 h, and then went up gradually for the short circuit photocurrent (J_{sc}) while the open circuit voltage (V_{oc}) continued to reduc slowly, resulting in a depression in solar cell efficiency for 28.5%. The unstability of the **DPP-II**-sensitized solar cell may be ascribed to the non-planarity of the dye structure, which probably could be desorbed easily from the TiO_2 surface and lead to faster electron transfer from TiO_2 to the electrolyte.

4. Conclusion

In summary, we have synthesized a new organic sensitizer **DPP-I** based on diketo-pyrrolo-pyrrole (DPP) containing a furan moiety as π-spacer for the application of dye-sensitized solar cells. **DPP-II** and **DPP-III** with a benzene and a thiophene linker, respectively, were also synthesized for the purpose of comparison. The introduction of furan and benzene linkers to tune the HOMO-LUMO levels increases the short circuit photocurrent (J_{sc}) and reaches higher efficiency. The cell based on the furan (**DPP-I**) and benzene (**DPP-II**) linkers exhibit 5.65% and 6.03% conversion efficiency, which are higher than that of **DPP-III** with the thiophene moiety. The solvent-free ionic liquid electrolyte solar cell was also tested and **DPP-I** exhibited better conversion efficiency of 4.41% and higher stability over 2000 h at full sunlight. Our findings demonstrate that the furan moiety can be advantageously incorporated into the dye-sensitizer as a π-spacer and even more efficient and stable than a thiophene moiety. Therefore, we conclude that the introduction of the renewable and sustainable furan moiety into the dye-sensitizer can both improve the cell efficiency and stability, and it would allow for a production of DSSCs on a large scale.

Acknowledgments

This work was supported by NSFC/China (21172073 and 61006048), the Fundamental Research Funds for the Central Universities (WJ0913001 and WJ1014025), Ph. D. Programs Foundation of Ministry of Education of China (20090074110004) and Scientific Committee of Shanghai (10520709700).

References

[1] O'Regan B, Grätzel M. A low-cost, high-efficiency solar cell based on dye-sensitized colloidal titanium dioxide films. Nature 1991;353:737–40.
[2] (a) Gao F, Wang Y, Zhang J, Shi D, Wang M, Humphry-Baker R, et al. A new heteroleptic ruthenium sensitizer enhances the absorptivity of mesoporous titania film for a high efficiency dye-sensitized solar cell. Chem Commun; 2008:2635–7;
(b) Yum JH, Jung I, Baik C, Ko J, Nazeeruddin MK, Grätzel M. High efficient donor–acceptor ruthenium complex for dye-sensitized solar cell applications. Energy Environ Sci 2009;2:100–2.
[3] Han LY, Fukui A, Chiba Y, Islam A, Komiya R, Fuke N, et al. Integrated dye-sensitized solar cell module with conversion efficiency of 8.2%. Appl Phys Lett 2009;94:013305.
[4] (a) Tang J, Wu WJ, Hua JL, Li J, Tian H. Starburst triphenylamine-based cyanine dye for efficient quasi-solid-state dye-sensitized solar cells. Energy Environ Sci 2009;2:982–90;
(b) Sayama K, Hara K, Ohga Y, Shinpou A, Suga S, Arakawa H. Significant effects of the distance between the cyanine dye skeleton and the semiconductor surface on the photoelectrochemical properties of dye-sensitized porous semiconductor electrodes. New J Chem 2001;25:200–2;
(c) Ma XM, Hua JL, Wu WJ, Tian H. A high-efficiency cyanine dye for dye-sensitized solar cells. Tetrahedron 2008;64:345–50.
[5] (a) Khazraji AC, Hotchandani S, Das S, Kamat PV. Controlling dye (merocyanine-540) aggregation on nanostructured TiO_2 films. An organized assembly approach for enhancing the efficiency of photosensitization. J Phys Chem B 1999;103:4693–700;
(b) Sayama K, Hara K, Mori N, Satsuki M, Suga S, Tsukagoshi S, et al. Photosensitization of a porous TiO_2 electrode with merocyanine dyes containing a carboxyl group and a long alkyl chain. Chem Commun; 2000:1173–4.
[6] (a) Wang ZS, Cui Y, Yasufumi D, Kasada C, Shinpo A, Kohjiro HK. Thiophene-functionalized coumarin dye for efficient dye-sensitized solar cells: electron lifetime improved by coadsorption of deoxycholic acid. J Phys Chem C 2007; 111:7224–30;
(b) Alibabaei L, Kim J-H, Wang M, Pootrakulchote N, Teuscher J, Censo D, et al. Molecular design of metal-free D–π-A substituted sensitizers for dye-sensitized solar cells. Energy Environ Sci 2010;3:1757–64.
[7] Hara K, Wang ZS, Cui Y, Furube A, Koumura N. Long-term stability of organic–dye-sensitized solar cells based on an alkyl-functionalized carbazole dye. Energy Environ Sci 2009;2:1109–14.
[8] Horiuchi T, Miura H, Sumioka K, Uchida S. High efficiency of dye-sensitized solar cells based on metal-free indoline dyes. J Am Chem Soc 2004;126: 12218–9.
[9] (a) Stathatos E, Lianos P. Synthesis of a hemicyanine dye bearing two carboxylic groups and its use as a photosensitizer in dye-sensitized photoelectro chemical cells. Chem Mater 2001;13:3888–92;
(b) Wang ZS, Li FY, Huang CH. Highly efficient sensitization of nanocrystalline TiO_2 films with styryl benzothiazolium propylsulfonate. Chem Commun; 2000:2063–4.
[10] Kitamura T, Ikeda M, Shigaki K, Inoue T, Anderson NA, Ai X, et al. Phenyl-conjugated oligoene sensitizers for TiO_2 solar cells. Chem Mater 2004;16: 1806–12.
[11] Hara K, Horiguchi T, Kinoshita T, Sayama K, Sugihara H, Arakawa H. Highly Efficient Photon-to-electron conversion of mercurochrome-sensitized nanoporous ZnO solar cells. Chem Lett 2000;29:316–8.
[12] (a) Tian HN, Yang XC, Chen RK, Pan YZ, Li L, Hagfeldt A, et al. Phenothiazine derivatives for efficient organic dye-sensitized solar cells. Chem Commun; 2007:3741–3;
(b) Wu WJ, Yang JB, Hua JL, Tang J, Zhang L, Long YT, et al. Efficient and stable dye-sensitized solar cells based on phenothiazine sensitizers with thiophene units. J Mater Chem 2010;20:1772–9.
[13] Tian HN, Yang XC, Chen RK, Hagfeldt A, Sun LC. A metal-free "black dye" for panchromatic dye-sensitized solar cells. Energy Environ Sci 2009;2:674–7.
[14] Zeng WD, Cao YM, Bai Y, Wang YH, Shi YS, Zhang M, et al. Efficient dye-sensitized solar cells with an organic photosensitizer featuring orderly conjugated ethylenedioxythiophene and dithienosilole blocks. Chem Mater 2010;22:1915–25.
[15] Goncalves LM, Bermudez VZ, Ribeiro HA, Mendes AM. Dye-sensitized solar cells: a safe bet for the future. Energy Environ Sci 2008;1:655–67.
[16] Yum J-H, Hagberg D, Moon S-J, Karlsson KM, Marinado T, Sun LC, et al. A light-resistant organic sensitizer for solar-cell applications. Angew Chem Int Ed 2009;48:1576–80.
[17] Tang J, Hua JL, Wu WJ, Li J, Jin ZG, Long YT, et al. New starburst sensitizer with carbazole antennas for efficient and stable dye-sensitized solar cells. Energy Environ Sci 2010;3:1736–45.
[18] Li C, Yum J-H, Moon S-J, Herrmann A, Eickemeyer F, Pschirer NG, et al. An improved perylene sensitizer for solar cell applications. ChemSusChem 2008; 1:615–8.
[19] Katoh R, Furube A, Mori S, Miyashita M, Sunahara K, Koumuraa N, et al. Highly stable sensitizer dyes for dye-sensitized solar cells: role of the oligothiophene moiety. Energy Environ Sci 2009;2:542–6.
[20] Qu SY, Wu WJ, Hua JL, Kong C, Long YT, Tian H. New diketopyrrolo-pyrrole (DPP) dyes for efficient dye-sensitized solar cells. J Phys Chem C 2010;114: 1343–9.

[21] Wang ZS, Cui Y, Dan-oh Y, Kasada C, Shinpo A, Hara K. Molecular design of coumarin dyes for stable and efficient organic dye-sensitized solar cells. J Phys Chem C 2008;112:17011–7.
[22] Zhu WH, Wu YZ, Wang ST, Li X, Chen J, Wang Z-S, et al. Organic D-A-π-A solar cell sensitizers with improved stability and spectral response. Adv Funct Mater 2011;21:756–63.
[23] Bunz UF. α-Oligofurans: molecules without a twist. Angew Chem Int Ed 2010; 49:5037–40.
[24] (a) Walker B, Tamayo AB, Dang X-D, Zalar P, Seo JH, Garcia A, et al. Nanoscale phase separation and high photovoltaic efficiency in solution-processed, small-molecule bulk heterojunction solar cells. Adv Funct Mater 2009;19: 3063–9;
(b) Yamamoto T, Zhou Z-H, Kanbara T, Shimura M, Kizu K, Maruyama T, et al. π-Conjugated donor–acceptor copolymers constituted of π-excessive and π-deficient arylene units. Optical and electrochemical properties in relation to CT structure of the polymer. J Am Chem Soc 1996;118:10389–99;
(c) Araki Y, Wada T, Yoshikawa O, Sagawa T, Yoshikawa S, Imahor H. Synthesis and photophysical and photovoltaic properties of porphyrin–furan and –thiophene alternating copolymers. J Phys Chem C 2009;113: 10798–806.
[25] Lin JT, Chen P-C, Yen Y-S, Hsu Y-C, Chou H-H, Yeh M-CP. Organic dyes containing furan moiety for high-performance dye-sensitized solar cells. Org Lett 2009;11:97–100.
[26] Woo CH, Beaujuge PM, Holcombe TW, Lee OP, Frechet JJ. Incorporation of furan into low band-gap polymers for efficient solar cells. J Am Chem Soc 2010;132:15547–9.
[27] Bijleveld JC, Karsten BP, Mathijssen SJ, Wienk MM, Leeuwb DM, Janssen RJ. Small band gap copolymers based on furan and diketopyrrolopyrrole for field-effect transistors and photovoltaic cells. J Mater Chem 2011;21:1600–6.
[28] Ohtani B, Prieto-Mahaney OO, Li D, Abe R. What is Degussa (Evonik) P25? Crystalline composition analysis, reconstruction from isolated pure particles and photocatalytic activity test. J Photochem Photobiol A: Chem 2010;216:179.
[29] Wang ZS, Kawauchi H, Kashima T, Arakawa H. Significant influence of TiO_2 photoelectrode morphology on the energy conversion efficiency of N719 dye-sensitized solar cell. Coordination Chem Rev 2004;248:1381–9.
[30] Nazeeruddin MK, Pechy P, Renouard T, Zakeeruddin SM, Humphry-Baker R, Comte P, et al. Engineering of efficient panchromatic sensitizers for nano-crystalline TiO_2-based solar cells. J Am Chem Soc 2001;123:1613–24.
[31] (a) Ning ZJ, Zhang Q, Wu WJ, Pei HC, Liu B, Tian H. Starburst triarylamine based dyes for efficient dye-sensitized solar cells. J Org Chem 2008;73: 3791–7;
(b) Ning Z, Fu Y, Tian H. Improvement of dye-sensitized solar cells: what we know and what we need to know. Energy Environ Sci 2010;3:1170–81.
[32] Teng C, Yang XC, Yang C, Li SF, Cheng M, Hagfeldt A, et al. Molecular design of anthracene-bridged metal-free organic dyes for efficient dye-sensitized solar cells. J Phys Chem C 2010;114:9101–10.
[33] Horiuchi T, Miura H, Uchidab S. Highly-efficient metal-free organic dyes for dye-sensitized solar cells. Chem Commun; 2003:3036–7.
[34] Mishra A, Fischer MK, Bauerle P. Metal-free organic dyes for dye-sensitized solar cells: from structure: property relationships to design rules. Angew Chem Int Ed 2009;48:2474–99.
[35] (a) Li RZ, Shi D, Zhou DF, Cheng YM, Zhang GL, Wang P. Dye-sensitized solar cells based on organic sensitizers with different conjugated linkers: furan, bifuran, thiophene, bithiophene, selenophene, and biselenophene. J Phys Chem C 2009;113:7469–79;
(b) Preat J, Jacquemin D, Perp EA. Towards new efficient dye-sensitised solar cells. Energy Environ Sci 2010;3:891–904.
[36] Teng C, Yang XC, Chao Y, Tian HN, Li SF, Wang XN, et al. Influence of triple bonds as π-spacer units in metal-free organic dyes for dye-sensitized solar cells. J Phys Chem C 2010;114:11305–13.
[37] Yum J-H, Jang SR, Walter P, Geiger T, Nuesch F, Kim S, et al. Efficient co-sensitization of nanocrystalline TiO_2 films by organic sensitizers. Chem Commun; 2007:4680–2.
[38] (a) Han LY, Koide N, Chiba Y, Islam A, Komiya R, Fuke N, et al. Improvement of efficiency of dye-sensitized solar cells by reduction of internal resistance. Appl Phys Lett 2005;86:213501–3;
(b) Wang Q, Moser J-E, Grätzel M. Electrochemical impedance spectroscopic analysis of dye-sensitized solar cells. J Phys Chem B 2005;109:14945–53;
(c) Han LY, Koide N, Chiba Y, Mitate T. Modeling of an equivalent circuit for dye-sensitized solar cells. Appl Phys Lett 2004;84:2433.
[39] Kuang DB, Uchida S, Humphry-Baker R, Zakeeruddin SM, Grätzel M. Organic dye-sensitized ionic liquid based solar cells: remarkable enhancement in performance through molecular design of indoline sensitizers. Angew Chem Int Ed 2008;47:1923–7.
[40] Qin H, Wenger S, Xu MF, Gao FF, Jing XY, Wang P, et al. An organic sensitizer with a fused dithienothiophene unit for efficient and stable dye-sensitized solar cells. J Am Chem Soc 2008;130:9202–3.
[41] Zhang G-L, Bai Y, Li R, Shi D, Wenger S, Zakeeruddin SM, et al. Employ a bis-thienothiophene linker to construct an organic chromophore for efficient and stable dye-sensitized solar cells. Energy Environ Sci 2009;2:92–5.